Real Time Adaptive RF and Digital Self-Interference Cancellation for Full-Duplex Transceivers

Visa Tapio, Markku Juntti, Aarno Pärssinen and Kari Rikkinen
Centre for Wireless Communications
University of Oulu, Finland
Email: firstname.lastname@oulu.fi

***Abstract*—The challenges with full-duplex (FD) transceiver implementation and transmission in small area radio communication systems are considered. The main challenge in the FD transceiver design is the self-interference (SI). Analog and digital SI cancellation is used for SI mitigation. Analog SI isolation is performed at radio frequency (RF) by utilizing an antenna design based on the characteristic modes theory and using active cancellation principle. Phase and attenuation values of the active cancellation signal path are tuned using a variable-step steepest descent algorithm while transmitting a data signal to a distant node in full-duplex mode. After the tuning, the SI isolation at RF processing is 90 dB. The remaining SI is then cancelled at the baseband processing for which the an estimate of the SI channel is needed. The SI channel estimation is done in full-duplex mode. Because the receiver has full knowledge of the transmitted signal, no extra pilots are used for the SI cancellation.**

***Index terms* – Full-duplex, self-interference, adaptive cancellation.**

I. Introduction

Full-duplex (FD) transceivers can transmit and receive simultaneously at the same carrier frequency offering the potential to double the spectral efficiency, to reduce air interface delays, and to facilitate improved collision detection and avoidance mechanisms in content based networks [1]. Therefore, FD transmission concept is identified as one possible technique for 5G systems [2], [3]. Other benefits as well as challenges in FD systems development have been reviewed in, e.g., [4], [5], [6], [7], [8].

The main problem in the FD transceiver design is the self-interference (SI), i.e., the leakage of the transmit signal to the device's own receiver. Depending on the system, the SI cancellation requirement can be well over 100 dB. In order to achieve such a high isolation levels, the SI cancellation must be done at different stages. Reviews on different SI cancellation techniques can be found, e.g., in [3], [9], [10]. In this paper, the self-interference cancellation is performed with three techniques: antenna isolation, active cancellation at radio frequency (RF) and digital cancellation at the baseband. Since the attenuation and phase settings of the active cancellation can change during the operation, they must be tunable. The usage of a gradient descent algorithm for the tuning has been proposed in [11]. Recent designs reported in [12], [13] also use iterative algorithms to adjust the phase and attenuation in the feed forward paths of the analog SI cancellers. The tuning of the SI cancellation in [11], [12], [13] is done prior the full-duplex communication. Designs in [12], [13] are independent front end designs, the tuning algorithms are run on a specific control unit and an additional analog-to-digital (AD) conversion is needed for the SI cancelation. In this work, the tuning of the active cancellation circuitry is done in the full-duplex (HD) mode using the transmitted data signal without the need to use a specific tuning signal, i.e., the data transmission can be continuous. All the processing is done at the baseband processing unit, hence no additional AD converters are needed for the SI cancellation.

The remaining SI after the first cancellation stage is cancelled at the baseband. Therein the SI channel is first estimated. The SI channel estimate and the known transmitted signal are then used to form a signal that is subtracted from the received signal. The SI channel estimation is performed during the reception of the signal from a distant node using the transmitted data signal. Hence, neither additional pilot symbols nor silent periods are needed for the SI channel estimation [14].

The rest of the paper is organized as follows. The transceiver model and the SI cancellation are described in Section II and numerical results are presented in Section III. Finally, conclusions are presented in Section IV.

II. Transceiver model and self-interference cancellation

The antenna design is based on the characteristic modes theory [15], [16]. The antenna offers 61 dB isolation over 20 MHz bandwidth. For the RF cancellation, an additional signal path consisting of a phase shifter (ϕ) and attenuator (Att) is added in parallel to the antenna to provide additional isolation, see Fig. 1. Port P1 is the transmitter's antenna port and P2 is the receiver's antenna port. Power splitter after P1 is used to sample the transmitted signal for analog SI isolation. The signal power fed to the phase shifter is 20 dB lower than that at port P1 and 99% of the power is propagating to the antenna. The power splitter can be implemented, e.g., as a 20 dB directional coupler. The power combiner before P2 is used to sum up the SI signal and the output signal of the attenuator. The signal from the attenuator is further attenuated by 20 dB

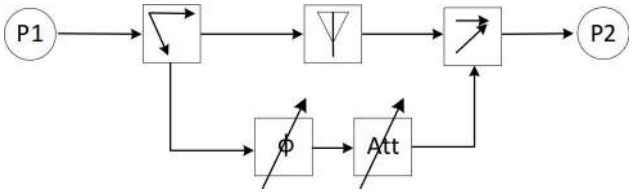

Fig. 1. Antenna and active cancellation.

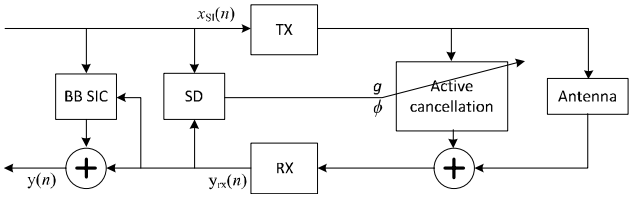

Fig. 2. Tuning of the active cancellation and BB SIC.

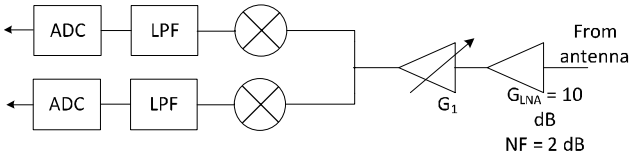

Fig. 3. Direct conversion receiver.

in the power combiner and it can be also be implemented as a directional coupler.

Because the SI path from the transmitter to the receiver can change during the communication the phase and attenuation of the SI isolation path must be tunable. The tuning of the SI isolation path is done using the transmitted data signal. The principle of the tuning is illustrated in Fig. 2. The phase and attenuation of the feed forward path are calculated iteratively using a variable-step deepest descent (SD) algorithm. At each iteration step a complex coefficient $w(k)$ is calculated as

$$w(k) = w(k-1) - \frac{\beta_i}{M\sqrt{P_x P_{rx}}} \sum_{n=1}^{M} y_{rx}(n) x_{SI}^*(n), \quad (1)$$

where k is the iteration index, M is the number of samples per iteration, P_x is the power of the SI signal x_{SI} at the baseband, P_{rx} is the power of the received signal y_{rx} at the baseband and β_i is the step size. The phase (ϕ) and attenuation (g) values for the feed forward path are calculated from the $w(k)$ as

$$g(k) = Q\{10 \cdot \log_{10} |w(k)|\} \quad (2)$$

$$\phi(k) = Q\{\arctan \frac{\Im(w(k))}{\Re(w(k))}\}, \quad (3)$$

where $Q\{\cdot\}$ is quantization operation. The phase and gain values are quantized because attenuators and phase shifters are typically controlled in fixed steps. The values of the attenuator and phase shifter are initialized at the beginning of the tuning process as $g(0)$ and $\phi(0)$, respectively. The initial value of coefficient w is

$$w(0) = |10^{g(0)/10}| \cdot e^{j\phi(0)}. \quad (4)$$

After each iteration the absolute value of the sample cross correlation $c(k)$ between the transmitted SI signal and the received signal is calculated as [17]

$$|c(k)| = |R_{xy}(k-N)|, \text{where} \quad (5)$$
$$R_{xy}(k) = \sum_{i=0}^{N-k-1} x_{SI}(i+k) y_{rx}^*(i).$$

The selection of the step size β_i and the decision to stop the tuning process is done based on Eq. 5. The tuning is started with a large step size for fast initial convergence. When the SI cancellation performance does not improve any more with the initial step size, a new smaller step size is used in following iterations (Algorithm 1). The step size reduction is performed until the smallest step is used, after which the tuning stops.

Algorithm 1. Variable step SD algorithm for analog SIC tuning.

if $\max|c(k)| < \max|c(k-1)|$ and $\alpha = 0$ **then**
  Update $g(k)$ and $\phi(k)$ using Eqs. (1), (2) and (3) with $\beta = \beta_0$
else if $\max|c(k)| \geq \max|c(k-1)|$ and $\alpha = 0$ **then**
  Update $g(k)$ and $\phi(k)$ using Eqs. (1), (2) and (3) with $\beta = \beta_1$ and
  update $\alpha = \alpha + 1$
else if $\max|c(k)| < \max|c(k-1)|$ and $\alpha = 1$ **then**
  Update $g(k)$ and $\phi(k)$ using Eqs. (1), (2) and (3) with $\beta = \beta_1$
else if $\max|c(k)| \geq \max|c(k-1)|$ and $\alpha = 1$ **then**
  Update $g(k)$ and $\phi(k)$ using Eqs. (1), (2) and (3) with $\beta = \beta_2$ and
  update $\alpha = \alpha + 1$
  ⋮
else if $\max|c(k)| < \max|c(k-1)|$ and $\alpha = \alpha_{\max}$ **then**
  Update $g(k)$ and $\phi(k)$ using Eqs. (1), (2) and (3) with $\beta = \beta_{\min}$
else
  stop
end if

The RX block in Fig. 2 is a direct conversion receiver with 12-bit AD converters (Fig. 3). The low noise amplifier gain and noise figure used in simulations are 10 dB and 2 dB, respectively. The variable gain amplifier (G1) is used to scale the signal power before the AD conversion.

The residual SI after the RF cancellation is further reduced with baseband processing as shown in Fig. 2. The SI channel is estimated as

$$\hat{\mathbf{h}}_{SI} = \mathbf{R}_x^{-1}\mathbf{r}, \quad (6)$$

TABLE I
PHASE NOISE.

Freq. offset	Phase noise
1 kHz	−87 dBc
10 kHz	−103 dBc
100 kHz	−99 dBc
1 MHz	−112 dBc

where $\mathbf{R}_x$ is the estimate of the autocorrelation matrix of the transmitted self-interference ($\mathbf{x}_{SI}$) and $\mathbf{r}$ is the vector of estimated cross-correlations between the received signal after the SI cancellation $y(n)$ and $x_{SI}(n)$.

The SI channel estimate is used to form a replica of the remaining SI signal, which is then subtracted from the received baseband signal. The signal after the baseband SI cancellation is then

$$\mathbf{y} = \mathbf{y}_\mathrm{d} + \mathbf{X}_\mathrm{SI}(\mathbf{h}_\mathrm{SI} - \hat{\mathbf{h}}_\mathrm{SI}) + \mathbf{n}. \quad (7)$$

After the SI cancellation, synchronization, channel estimation and data detection are performed for the desired signal. Channel for the desired signal is estimated utilizing the long training sequence (LTS) of the IEEE 802.11 [18]. The channel estimate at sub-carrier k is [19]

$$h_k = \frac{1}{2}(y_{1,k} + y_{2,k})x_k^*, \quad (8)$$

III. NUMERICAL RESULTS

The signal used in simulations is an orthogonal frequency-division multiplexing (OFDM) signal with 48 data sub-carriers and 4 pilot sub-carriers at 3.5 GHz center frequency. Data sub-carriers are modulated using 16 level quadrature amplitude modulation (16-QAM). The bandwidth of the signal is 20 MHz. The antenna is modelled using an electromagnetic simulation tool (CST Microwave Studio). Simulated S-parameters are brought to the system model as a S-parameter file. The isolation of the antenna over the signal bandwidth is shown in Fig. 4. The solid red curve shows the isolation in decibels (dB) and the dashed blue curve shows the phase response in degrees (°). The FD transceiver including the analog SI isolation and AD converters is modelled using the Advanced Design System (ADS). The maximum values of the integral (INL) and differential (DNL) non-linearity to least significant bit of the AD converters are 5.0 and 0.7, respectively. The phase and amplitude imbalance of the transceivers are 0.5° and 0.1 dB, respectively, and the phase noise is given in Table I [20]. The non-linearity of power amplifiers is characterized with output 1 dB compression point (P_{1dB}) and third order intercept point (OIP_3) using the amplifier model available in ADS [21]. The $P_{1\mathrm{dB}}$ is set 6 dB above the average transmit power and $OIP_3 = P_{1\mathrm{dB}} + 10$ dB.

Baseband signal generation and the baseband FD receiver including the control of the analog SI isolation are implemented using Matlab. The starting point for the Matlab model development has been the OFDM simulation model from [22]. Baseband and RF models are included in the same simulation

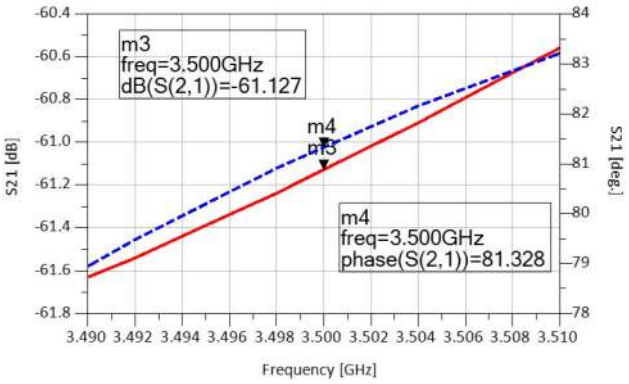

Fig. 4. Antenna isolation.

model allowing to model the interplay between the RF and baseband domains. Examples of the tuning performance are shown in Figs. 5 and 6. In the case of Fig. 5, the initial values of the attenuator and phase shifter are −15 dB and 0°, respectively and in Fig. 6 the initial values are −15 dB and 120°. Two step sizes are used in Algorithm 1 and they are $\beta_0 = 5 \cdot 10^{-3}$ and $\beta_1 = 1 \cdot 10^{-3}$. The blue curves show the performance when the attenuation tuning resolution is 1 dB. Red curves shows the performance when the attenuation resolution is decreased to 0.5 dB and magenta curves show the performance when the tuning resolution is further decreased to 0.25 dB. The phase tuning resolution is 5° in all the cases. As can be seen from Figs. 5 and 6 the performance of the analog SI cancellation after the tuning varies depending on the difference between the initial and optimal values of the attenuator and phase shifter. With further simulations it was found out that when the initial attenuator value is −15 dB and the initial phase shifter value is changed between $0 - 360°$ the SI cancellation performance changes from 78 to 90 dB with 1 dB attenuation resolution, with 0.25 dB resolution the SI cancellation performance is $90 - 94$ dB and with 0.5 dB resolution it is 90 dB. These SI cancellation values include the 61 dB isolation provided by the antenna. Hence, the additional SI attenuation provided by the active cancellation is between 17 and 33 dB and it is achieved after less than 15 iterations. One iteration equals the transmission of 25 OFDM symbols. Results in Figs. 5 and 6 are from a case when the tuning is done in HD mode. The tuning in FD mode converges to the same attenuator and phase shifter values with similar number of iterations, i.e., the tuning performance is the same in the FD and HD modes.

Bit error rate (BER) performance of an un-coded FD link was also evaluated. In BER simulations the initial phase and attenuation values of the analog SI have been 0° and −15 dB and the phase and attenuation resolution in the tuning phase have been 5° and 0.5 dB, respectively. BER measurement has started after the tuning of the analog SI cancellation has converged. BER results for the additive white Gaussian noise channel (AWGN) case and for a non-line of sight (NLOS) indoor channel case are shown if Figs. 7 and 8,

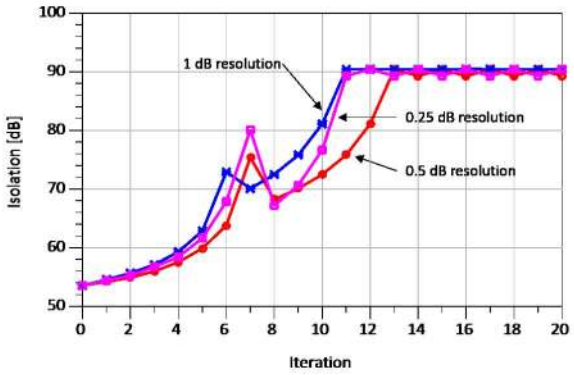

Fig. 5. Analog SI cancellation, initial phase 0°.

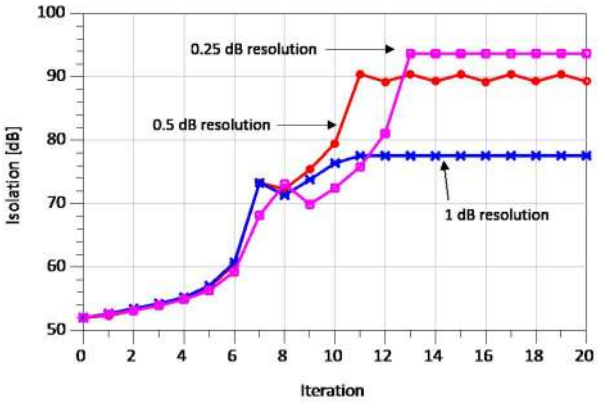

Fig. 6. Analog SI cancellation, initial phase 120°.

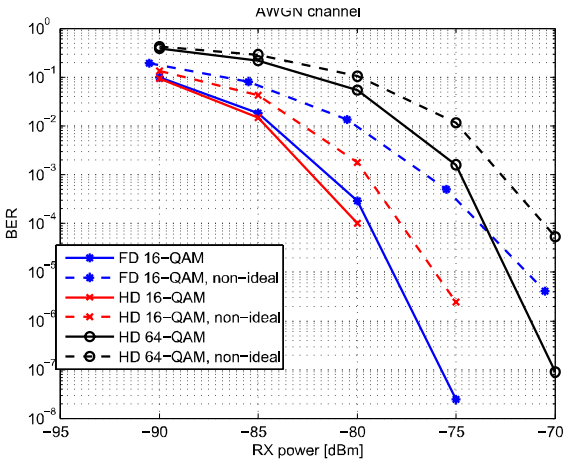

Fig. 7. BER in AWGN channel.

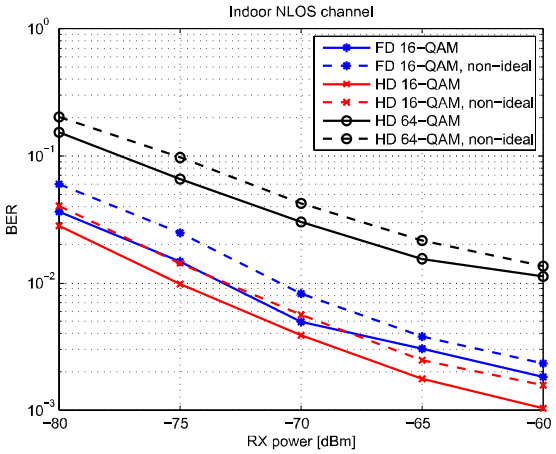

Fig. 8. BER in NLOS channel.

respectively. The NLOS channel model used in simulations is the Hiperlan/2 model A [21]. The blue curves show the performance of the FD link with 16-QAM modulation and the red curve shows the performance of the 16-QAM HD link (i.e., no self-interference). For comparison, the BER performance of a 64-QAM HD link is also simulated. Solid lines give the performance with ideal transceivers and dashed lines show the performance when the transceivers' non-ideal operation is modeled with the parameters given above. As can be seen from Figs. 7 and 8 the HD link with 64-QAM modulation requires more than 5 dB higher transmission power to reach the same BER performance than the 16-QAM FD link.

IV. Conclusions

Analog and SI cancellation was considered. Antenna design based on the characteristic modes theory provides 61 dB isolation. The isolation at RF is further increased by utilizing a feed-forward path from the transmitter's power amplifier output to the receiver's low-noise amplifier input. The attenuation and phase shift of the feed-forward path must be accurately tuned in order to gain the additional SI isolation. The tuning is performed in a HD mode using the transmitted signal and the variable step steepest descent algorithm. After the tuning up to 33 dB additional isolation is gained resulting in total RF isolation of 94 dB. The residual self-interference is cancelled by estimating the SI channel using the transmitted data signal. The estimated SI channel is then used to form an estimate of the residual SI which is subsequently subtracted from the received signal. After the synchronization, channel estimation an data detection of the desired signal the BER is used to measure the FD link performance. As expected, the 16-QAM HD link does not achieve the same BER performance as a 16-QAM HD link due to the residual SI after the baseband SI cancellation, i.e., the FD does not double the information theoretic channel capacity of a HD system. However, the 64-QAM HD link, that offers 1.5 times the capacity of a 16-QAM HD link, requires more than 5 dB higher transmission power than the 16-QAM FD link to achieve the same BER performance than the 16-QAM FD link.

As mentioned above, FD communications can enhance the spectral efficiency of wireless networks and thus, is a potential candidate for 5G. Besides, FD transceivers can support simultaneous uplink and downlink traffic, which can also be used for in-band wireless backhaul applications as pointed out in [4]. Furthermore, another promising application for FD

transceivers is in relay networks, which is closer to a practical scenario, since terminal nodes would be HD, while the base station is FD as evinced in [1] as well as in [23].

ACKNOWLEDGMENT

Antenna s-parameter files were provided by Dr. Marko Sonkki, Centre for Wireless Communications.

This work has been funded by Tekes - the Finnish Funding Agency for Innovation, Nokia Oyj, Esju Oy and CoreHW Oy.

REFERENCES

[1] K. Rikkinen, V. Tapio, H. Alves, M. Al-Imari, A. C. Cirik, J. Seddar, A. Sethi, B. Debaillie, and C. Lavin, "Full-duplex transmission in small area radio communication systems," in *2015 IEEE 20th International Workshop onComputer Aided Modelling and Design of Communication Links and Networks (CAMAD)*, Sept 2015, pp. 1–5.

[2] "NGMN 5G white paper," Next Generation Mobile Networks (NGMN) Alliance, Tech. Rep., February 2015.

[3] Z. Zhang, X. Chai, K. Long, A. V. Vasilakos, and L. Hanzo, "Full duplex techniques for 5g networks: self-interference cancellation, protocol design, and relay selection," *IEEE Communications Magazine*, vol. 53, no. 5, pp. 128–137, May 2015.

[4] G. Liu, F. R. Yu, H. Ji, V. C. M. Leung, and X. Li, "In-band full-duplex relaying: A survey, research issues and challenges," *IEEE Communications Surveys Tutorials*, vol. 17, no. 2, pp. 500–524, Secondquarter 2015.

[5] S. Hong, J. Brand, J. I. Choi, M. Jain, J. Mehlman, S. Katti, and P. Levis, "Applications of self-interference cancellation in 5g and beyond," *IEEE Communications Magazine*, vol. 52, no. 2, pp. 114–121, February 2014.

[6] D. Kim, H. Lee, and D. Hong, "A survey of in-band full-duplex transmission: From the perspective of phy and mac layers," *IEEE Communications Surveys Tutorials*, vol. 17, no. 4, pp. 2017–2046, Fourthquarter 2015.

[7] A. Sabharwal, P. Schniter, D. Guo, D. W. Bliss, S. Rangarajan, and R. Wichman, "In-band full-duplex wireless: Challenges and opportunities," *IEEE Journal on Selected Areas in Communications*, vol. 32, no. 9, pp. 1637–1652, Sept 2014.

[8] M. Juntti, K. Rikkinen, B. Debaillie, C. Lavin, M. Ghoraishi, and V. Tapio, "Full duplexing," in *5G Wireless Technologies*, A. Alexiou, Ed. IET Publishing, ch. 7, due: February 2017.

[9] M. Heino, D. Korpi, T. Huusari, E. Antonio-Rodriguez, S. Venkatasubramanian, T. Riihonen, L. Anttila, C. Icheln, K. Haneda, R. Wichman, and M. Valkama, "Recent advances in antenna design and interference cancellation algorithms for in-band full duplex relays," *IEEE Communications Magazine*, vol. 53, no. 5, pp. 91–101, May 2015.

[10] B. Debaillie, D. J. van den Broek, C. Lavn, B. van Liempd, E. A. M. Klumperink, C. Palacios, J. Craninckx, B. Nauta, and A. Prssinen, "Analog/rf solutions enabling compact full-duplex radios," *IEEE Journal on Selected Areas in Communications*, vol. 32, no. 9, pp. 1662–1673, Sept 2014.

[11] M. Jain and et al., "Practical, real-time, full duplex wireless," in *Proceedings of the 17th Annual International Conference on Mobile Computing and Networking (MobiCom '11)*. New York, NY, USA: ACM, 2011, pp. 301–312. [Online]. Available: http://doi.acm.org/10.1145/2030613.2030647

[12] T. Huusari, Y. S. Choi, P. Liikkanen, D. Korpi, S. Talwar, and M. Valkama, "Wideband self-adaptive rf cancellation circuit for full-duplex radio: Operating principle and measurements," in *2015 IEEE 81st Vehicular Technology Conference (VTC Spring)*, May 2015, pp. 1–7.

[13] K. E. Kolodziej, J. G. McMichael, and B. T. Perry, "Multitap rf canceller for in-band full-duplex wireless communications," *IEEE Transactions on Wireless Communications*, vol. 15, no. 6, pp. 4321–4334, June 2016.

[14] V. Tapio and M. Sonkki, "Analog and digital self-interference cancellation for full-duplex transceivers," in *22th European Wireless Conference European Wireless 2016*, May 2016, pp. 1–5.

[15] R. Garbacz and R. Turpin, "A generalized expansion for radiated and scattered fields," *IEEE Transactions on Antennas and Propagation*, vol. 19, no. 3, pp. 348–358, May 1971.

[16] R. Harrington and J. Mautz, "Theory of characteristic modes for conducting bodies," *IEEE Transactions on Antennas and Propagation*, vol. 19, no. 5, pp. 622–628, Sep 1971.

[17] "Matlab documentation," The MathWorks, Inc., Manual.

[18] I. C. Society, "Part 11: Wireless LAN Medium Access Control (MAC) and Physical Layer (PHY) Specifications," IEEE, Standard, 2012.

[19] J. Heiskala and J. Terry, *OFDM Wireless LANs: A Theoretical and Practical Guide* . Sams Publishing.

[20] "MAX/2828/2829 Single-/Dual-Band 802.11 a/b/g World-Band Transceiver ICs," Maxim Integrated Products, Inc., Data sheet.

[21] "Ads documentation," Keysight Technologies Inc., Manual.

[22] R. University WARP project. http://warp.rice.edu.

[23] H. Alves, R. D. Souza, and M. E. Pellenz, "Brief survey on full-duplex relaying and its applications on 5g," in *2015 IEEE 20th International Workshop on Computer Aided Modelling and Design of Communication Links and Networks (CAMAD)*, Sept 2015, pp. 17–21.